Impacts on Multi-pulse Pulse Position Modulation Visible Light Communication from Outdoor Daylight Conditions

Don Barber
Naval Postgraduate School
don.barber@nps.edu

Christopher Pickle
Naval Postgraduate School
christopher.pickle@nps.edu

Zachary White
Naval Postgraduate School
zachary.white@nps.edu

Abstract

The growing deployment of light-emitting diodes as energy-efficient, cost-effective lighting for vehicles opens opportunities for visible light vehicle-to-vehicle communication. Leveraging existing headlights and taillights on cars for inter-vehicle communication offers an opportunity to save on both hardware costs and the use of the congested radio frequency spectrum. However, most vehicle-to-vehicle visible light communication investigations in the literature have been limited in range. This paper presents an overview of the factors impacting outdoor visible light communications at increasing distances and presents findings from outdoor testing at ranges approaching 200 m. Using software spatial filtering and multi-pulse pulse position modulation, strong throughput is shown at 50 m in daylight conditions, with improving symbol error rates achieved in outdoor daylight conditions at 100 m by increasing intensity modulation.

Keywords: Interference, Multi-pulse pulse position modulation, Optical camera communication, Visible light communication, Vehicle-to-vehicle communication

1. Introduction

An ever-increasing number of devices are competing for wireless spectrum to communicate. 5G cellular standards have expanded in scope beyond just higher cellular data rates to now also incorporate prolific internet of things (IoT) devices and prioritized low-latency traffic. One of the many applications of emerging device-to-device communications is vehicle-to-vehicle (V2V) communication. V2V communications can increase both safety and efficiency on roadways. Communications between cars can relay alerts of upcoming changes in traffic flow before drivers would otherwise be able to see or react to them. Ongoing regulatory efforts, including *Federal Motor Vehicle Safety Standards; V2V Communications* (2017), aim to codify standards to allow inter-vehicle communication. Common communications standards are needed to reach a critical mass of cars and benefit from the efficiencies of inter-vehicle communication. The Institute of Electrical and Electronics Engineers (IEEE) (2010) 802.11p standard prescribes 5.9 GHz radio frequency signaling to enable V2V communications.

Despite the promise of these efforts, spectrum remains a limited resource. A decade ago with the introduction of cost-effective light-emitting diode (LED) light fixtures, research began into visible light communications (VLC). VLC leverages existing illumination fixtures to transmit data while also continuing to provide functional lighting. More recently, vehicle lighting has also began transitioning to LED technology in earnest.

While the bulk of VLC research has focused on communications in controlled indoor environments, there is growing interest in outdoor VLC for V2V communication. Despite early progress in V2V VLC, Cailean and Dimian (2016) note that progress has been limited by challenges of range and weather. Several proof of concept LED V2V systems have been proposed in the literature, including Avatamanitei et al. (2020), Ji et al. (2014), Lourenco et al. (2012), and Yoo et al. (2016), but they have generally been limited in range to less than 50 meters. Rizzo et al. (2011) found dry pavement stopping distances from 100 km/h with anti-lock brakes are generally around 50 m, and increase as tires age. This suggests 50 m is really a minimum

URI: https://hdl.handle.net/10125/103430
978-0-9981331-6-4

acceptable range for V2V VLC.

This paper assesses the factors that impact the range of outdoor daytime VLC. Our experiments focus on outdoor VLC using a commodity complementary metal-oxide semiconductor (CMOS) sensor – a phone camera – as a receiver, similar to Ji et al. (2014). While providing significant receiver diversity gain over a single photodiode, CMOS sensors are inexpensive and ubiquitous, making them the most likely technology to be integrated into a vehicle subsystem. Previous work by Danakis et al. (2012) with cameras as sensors highlighted rolling shutter techniques to increase sample rate, but our work focuses on effects related to signal-to-noise ratio (SNR) at range rather than increasing the speed.

We leverage multi-pulse pulse position modulation (MPPM) as our base waveform, which has been proven to be robust by Koss et al. (2020) and White et al. (2022). Further, we assess spatial filtering within the frame to maintain sufficient SNR for communication at increasing ranges in ambient sunlight, a critical condition of V2V communication, as well as the impact of relative pulse modulation height. Previous work by Teli and Chung (2018) employed selective capture to increase speed in flicker-free V2V communication.

Finally, since flicker-free operation is a key aspect of VLC in order for luminaries to support their primary function while also transmitting data, a dimming constraint is specified to quantify visible changes in brightness. Cailean and Dimian (2017) noted that indoor VLC dimming thresholds are sometimes as tight as 0.1% of fixture brightness. Given the significantly higher amount of background noise in a daytime outdoor environment, we measured various dimming percentages to assess the impact on communication link stability.

This paper presents empirical measurements of an outdoor VLC transmission at varying ranges using spatial filtering in software to maintain sufficient SNR for communication. Section 2 provides an overview of the geometric effects of increasing range on VLC and other effects that decrease received signal and increase noise. Section 3 describes the experimental methodology used to assess the impacts of increasing range on VLC in daylight conditions, with experimental results captured in Section 4. Section 5 summarizes our findings and presents opportunities for further work.

2. Effects of Increasing Range on Outdoor VLC

V2V VLC imply a requirement for transmissions at ranges far greater than typical indoor VLC applications. In their paper summarizing the challenges of automotive VLC, Cailean and Dimian (2017) highlighted distance-dependent path loss and SNR as critical challenges. Ghassemlooy et al. (2019) offer that optical propagation is very similar to radio frequency line of sight communication, but there are dramatically more interactions between photons at optical wavelengths and atmospheric particles than there are at radio frequencies. This section explores the challenges and impacts of increasing range on VLC using camera sensors, also called optical camera communication (OCC).

2.1. Geometric Losses

Increasing range has two geometric effects reducing the signal energy at the camera image sensor. First, as distance increases, transmitting lights in a scene take up less space within the camera field of view (FOV), illuminating fewer pixel diodes. Compounding this loss of integration area, the light energy in the transmitted wavefront decays as a square of the distance from the source. In the fundamentals of communication theory developed by Shannon (1948), SNR is the defining parameter for the information capacity of a channel. Both the geometric effects of spreading and decreased area within the FOV reduce received signal power and in turn SNR.

Yamazato et al. (2015) suggested that a simplified pinhole camera model could be used to make calculations for V2V VLC, and SNR could be held constant by always selecting the brightest pixel in the received set. We begin our analysis here, leveraging a simplified camera model, but our results ultimately highlight that there is significant variation in atmosphere and quantization effects as range increases beyond a thin lens or pinhole camera model.

Consistently, as range increases the transmitting light occupies a smaller and smaller portion of the FOV of the receiving sensor. Assuming a simplified thin lens as an approximation of the camera optics, the object and its image on the sensor are related by similar triangles

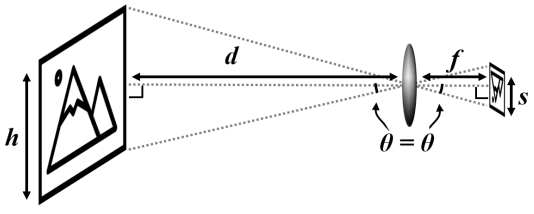

Figure 1. The same size object fills less of the camera sensor at increasing range.

as shown in Figure 1 where d is the distance from the camera to the object, h is the height of the object, f is the focal distance of the camera, and s is the height of the sensor. Given the equivalence of angles, tangent θ, the opposite over adjacent, must be equal:

$$\frac{h}{d} = \frac{s}{f}. \tag{1}$$

Since the size of the object and the focal length can be assumed constant, as distance increases the projected size of the image is expected to decrease linearly.

At the same time, as light energy propagates, it spreads in space, as illustrated in Figure 2. Considering a point source of light, at any distance from the source, the light energy is spread over the surface of a sphere with an area $4\pi r^2$. Of course, many sources will have some directional gain, such as a parabolic reflector behind the light, but the gain from directionalized light is a constant multiple of the initial field. Holding the 4π and gain factors constant, the far-field loss can be approximated simply as r^2 losses.

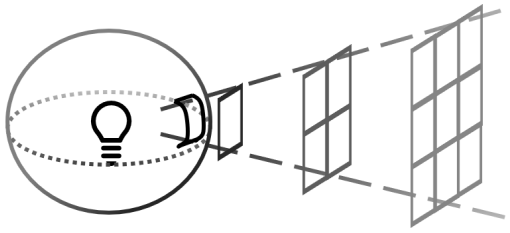

Figure 2. Illustration of the energy spreading as a factor of range squared.

Ultimately, these two loss effects result in a wavefront with less energy reaching fewer photosensor pixels, significantly attenuating signal in the signal-to-noise ratio.

2.2. Dynamic Range and Quantization Resolution

Due to the nature of transmitting LEDs and photodiodes in CMOS sensors, VLC generally depends on intensity modulation/direct detection techniques as employed in Yoo et al. (2016). In order to continue to support the illumination requirements of the vehicle fixture, such as daytime running lights, it is important not to generate perceptible flicker. Analogous to the indoor VLC scenario discussed in Cailean and Dimian (2017), limiting the intensity modulation to a small fraction of the total luminance value is significantly less perceptible than toggling the fixture completely on and off.

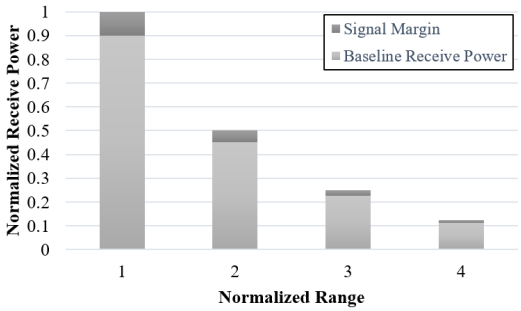

Figure 3. Decreasing signal margin with increasing range based on a 10% modulation factor.

However, limiting the dynamic range of the signal at the transmitter proportionally compresses the dynamic range of the signal at the receiver. Even before considering other noise sources, as the overall signal gets smaller, the change between high and low pulses also gets smaller as seen in the signal margin in Figure 3. Since the receiver is providing digital data out of the camera, it is necessarily quantized. Smaller and smaller signal delta means the change is compressed into fewer and fewer quantization bins. Increasing quantization noise alone makes the signal less discernible and it amplifies susceptibility to noise interference.

2.3. Other Camera Effects

Beyond quantization noise, OCC using commercially available cameras and their built-in software introduce many subtle artifacts designed to optimize the appearance of images that can create challenges receiving VLC with small margins. In order to generate color pictures, a tristimulus model based on three primary colors aligned to human visual sensitivity is used. Since the photoreceptors in CMOS cameras cannot themselves differentiate color, a pattern of color filters is set on top of the sensor. In a localized area one pixel sensor receives red, two receive green (which humans are most sensitive to), and one receives blue. To generate a final image, these adjacent pixels are mixed to produce the overall color value. While this is a simple and cost-effective way to generate visually pleasing images, pixel mixing adds distortion to the image. Shortis et al. (2005) and others have looked at approaches to minimize the impact of this color filter mosaic, but often the speed needed for video recording necessitates the use of simple, fast algorithms.

As with any sensor, there is also inherent electrical noise in the sensor and circuits themselves. Even off-axis sunlight not in the direct path from the image to the sensor tends to increase shot noise in the camera

sensor.

2.4. Atmospheric Scattering Noise

Beyond an increase in relative quantization noise and induced camera artifacts, increasing range also adds additional interference along the channel. Along the column of air between the transmitting light and receive sensor, atmospheric particles scatter both the signal light and other ambient light. The portion of the intended signal that is scattered further reduces the energy received beyond the drop from r^2 losses. Any additional ambient light that is scattered in the direction of the sensor adds to signal noise. Spatial filtering helps to reduce the diameter of the cone of interest, but also reduces the area on the sensor over which the received signal is integrated.

As distance increases, more atmospheric particles will be in the path generating these interactions and cause greater relative noise in the received signal. It is intuitive that adverse conditions, such as fog, would cause atmospheric path loss to be significant, but even in clear conditions a significant amount of sunlight is randomly scattered. Over long distances, this particle scattering makes the sky blue, turning to reds and oranges through even longer distances in the atmosphere at sunset. Even at short distances, there is appreciable scattering impacting the ability to differentiate intensity-modulated pulses.

3. Experimental Methodology

In order to assess range varying impacts on V2V VLC, we conducted tests using digital multiplex (DMX) controlled LED lights emulating car headlights at ranges from 12.5 m to 192 m, with limiting factors of building length and inter-building distance. Testing assessed the impacts of spatial filtering, increasing range, and varying the intensity of the modulation. This section outlines the hardware, physical layer encoding scheme, and test parameters.

3.1. Test Hardware

Testing was conducted using two LCP008S DMX lights spaced 1.5 m apart as surrogate vehicle lights. The LCP008S face has a diameter of 20 cm, with 54×1.5 W LED pixels controlled in unison by a DMX control box receiving control signals over a USB cable from a Raspberry Pi microcomputer programmed to modulate the lights as discussed in Section 3.2.

An iPhone 13 Pro Max was used as the receiving camera. The iPhone was set to record at 120 frames per second to ensure results would be reproducible with other commodity phone cameras. The iPhone, and even many inexpensive Android phones, can capture 240 frames per second to provide slow-motion playback, but 120 frames per second was most conservative since the goal of the study was to assess the effects of increasing range and not maximize throughput speeds.

While recording video, 3x optical zoom was used for all ranges. Optical zoom was used to maximize the relative integration area over the sensor, but as outlined by Sanyal (2021), the zoom sensor area is 12 mm^2 whereas the main sensor is 44 mm^2, creating a tradeoff. From Apple (2021), the iPhone telephoto camera has an effective focal length of 77 mm, but we also found that effective focal length is not a direct stand-in for the simplified focal length in Equation 1.

3.2. Physical Layer Encoding

Koss et al. (2020) and White et al. (2022) previously developed a set of orthogonal and uniquely decodable, MPPM codes that allow self-synchronization and mitigate challenges of frame synchronization in VLC. According to Rajagopal et al. (2012), MPPM is a common code for use in VLC as described in IEEE 802.15.7. Velidi and Georghiades (1995) noted that MPPM offers higher power efficiency than pulse width modulation (PWM) and higher spectral efficiency than pulse position modulation (PPM) for long symbols.

We chose a symbol set utilizing four pulses positioned in an overall symbol length of 26 time slots. The symbols were selected to have the largest possible Hamming distance from each other, in this case six, while preserving the self-synchronization property. Building on White et al. (2022), we chose to use a two-transmitter configuration, with each nominal headlight sending time-staggered symbols and their inverses and a single receiving camera to establish a basic (multiple-input, single-output) setup. This configuration added transmit diversity. A combiner scheme aided in further decreasing symbol error probability.

Symbols used 26 time slots, with four pulses included per symbol. The transmission time for a slot was set to $1/30$ s. With $26 \times 1/30$ s slots, the overall symbol transmission rate was 1.15 symbols/s. The 120 frames per second slow-motion video mode on the iPhone 13 was four times faster than our transmit time slot rate, and well above the minimum Nyquist sampling rate for these symbols.

Chowdhury et al. (2018) and others have studied OCC in detail, with a plethora of applications in the realm of VLC. Nonetheless, OCC still present some major challenges including low data rates (limited by

the camera frame rate as discussed) and the fact that they are traditionally one-way communications. Another key motivation for MPPM is the lack of a feedback loop for the receiver to communicate channel state information to the transmitter or send acknowledgments as are often used to optimize radio frequency communications.

The MPPM scheme with transmit diversity proposed by White et al. (2022) allows the receiver to estimate the channel state matrix from a known preamble which is used by the receiver to calculate needed equalization for the remainder of the transmission. This approach assumes the channel is static between pilot preambles and that there exists only slow, flat fading in the VLC channel. With our outdoor testing at ranges in excess of 100 m, we know wind buffeting of the exposed lights and cameras was causing physical variations so the transmitter and receiver were not stationary.

Using MPPM, ten symbols were sent during each test. Intensity modulation was performed digitally with PWM. The Raspberry Pi performed PWM using an 800 Hz clock, which was significantly faster than the camera exposure time and integrated smoothly to produce the overall desired intensity. In other experiments with much higher speed cameras (10x faster), it was possible to observe the peaks in PWM, but using OCC the CMOS integration over the sample period correctly produced the desired intensity modulation. The amplitude of modulation was controlled on a 0 to 255 scale for the DMX lights.

3.3. Test Configurations

Initial control testing was conducted indoors at a distance of 5 m, validating the performance of the hardware in Section 3.1 and the MPPM scheme in Section 3.2. Indoor, full-frame averaging of luminance values was sufficient to recover all ten transmitted symbols in MPPM with the transmit diversity scheme even at a low brightness modulation index due to the lack of interfering noise and (relatively) short range.

The DMX lights were attached to a metal rail on a wheeled cart hosting the controlling microcomputer and USB DMX controllers to allow outdoor positioning on a building rooftop. Inter-light spacing was set at 1.5 m to approximate the width of a small car. The iPhone 13 was fixed to a tripod for ease of mobility between range measures.

Outdoor testing to assess the impacts of range and spatial filtering was conducted in the late morning after the initial morning overcast had dispersed. Atmospheric conditions were 14° C, humidity 80%, and visibility of 16 km. Tests were conducted at increasing distances from the transmitters, as seen in Figure 4, at 12.5 m, 25 m, 50 m, and 140 m as limited by the length of the building. Immediately following these tests, the cart was repositioned and collection was conducted from the transmitter to the tower seen in Figure 5, a distance of 192 m (between buildings). Significant wind disturbance to the camera occurred at 140 m. After repositioning, the lights also received significant wind impacts during the 192 m test (note the blowing papers in Figure 5). These impacts exacerbated the effects of increasing range discussed in Section 2, but motion in scene is also a realistic challenge likely to be encountered in longer-range V2V VLC.

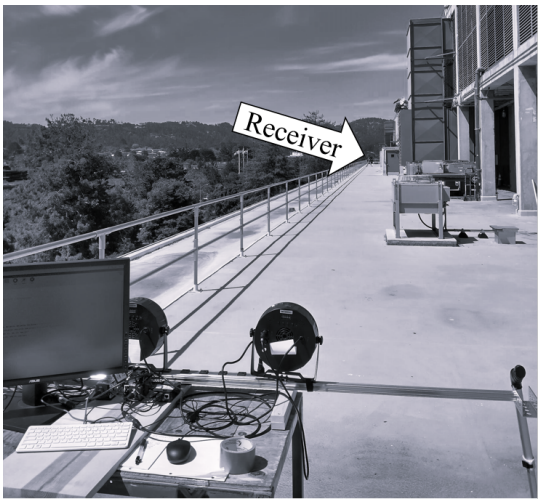

Figure 4. View from transmitter to collector at end of building (140 m).

Figure 5. View from transmitter to collector on tower (192 m).

Subsequently, outdoor testing was conducted to evaluate the impact of changing the intensity modulation delta. Modulation delta tests were conducted at 50 m

and 100 m in atmospheric conditions of 17° C, humidity 77%, and visibility of 16 km. Modulation deltas of 8%, 12%, 16%, 20%, 24%, 28%, 32%, 36%, 40%, 44%, 48%, 70% and 100% were used, with 100% providing full on/off signaling from the LEDs.

4. Results

4.1. Effects of Increased Range

As distance increased, the number of pixels illuminated by the transmitting lights initially fell off approximately linearly, as expected per Equation 1. However, as shown in Figure 6, as the range increased beyond 50 m, the rate of drop-off in pixel diameter actually decreased. Rather than halving as distance doubled, pixel diameter only fell off by a third each time distance doubled. This suggest a logarithmic fit may ultimately be a better model for estimated pixel height at range.

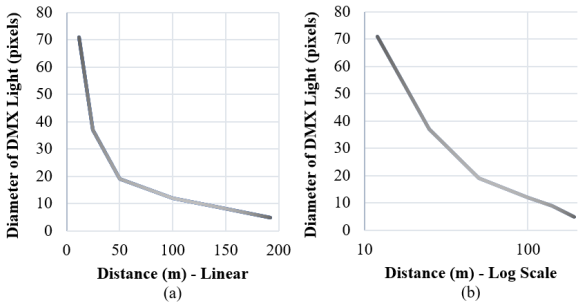

Figure 6. Diameter of light in image pixels vs range to the sensor on a linear scale (a) and logarithmic scale (b).

Beyond the simplifying thin lens assumption used in Equation 1, atmospheric dispersion, pixel mixing , and non-uniformities in the propagating optical wavefront become a major factor with low numbers of pixels. Figure 7 shows a zoomed-in view of the transmitting lights as imaged from the tower in Figure 5. The lights are no longer sharply confined to the faces of the DMX light but blurred and bloomed out across multiple adjacent pixels. Techniques to increase range may need to address some or all of these issues, including accessing raw CMOS sensor data before processing and applying correction via optics or deconvolution of the channel to spatially separate pixels containing signal from those that are only noise.

Following indoor calibration, initial tests for range variance included lower modulation indexes of 2.5% and 5%, we were unable to achieve any consistent results. For outdoor testing, we focused on measurements with a 10% modulation index. In daylight conditions from

Figure 7. Zoomed in view of transmitting lights at 192 m showing dispersion bloom.

a few feet away, flicker was minimal, falling off to being undetectable at the positions of the camera measurements. Very close to the lights, 10% intensity modulation with a time slot of $1/30$ did produce some perceptible artifacts, but 10% seemed to be a reasonable trade-off with no noticeable flicker at range and still allowing some throughput.

Similarly, while full-frame luminance averaging was effective indoors, it did not work in daylight conditions. The amount of random variation across the full CMOS sensor completely overwhelmed the signal in all cases. Applying a spatial filter to only process the pixels in a box around each light matching the pixel heights seen in Figure 6 drastically improved the pulse to ambient noise SNR before any additional signal processing, as can be seen in Figure 8. Even at our minimum range of 12.5 m, in Figure 8(a) noise completely overwhelms the signal, whereas after applying a spatial filter to limit the area of interest to just the transmitting lights in Figure 8(b), the pulses can clearly be seen even amid the baseline drift and other pattern noise.

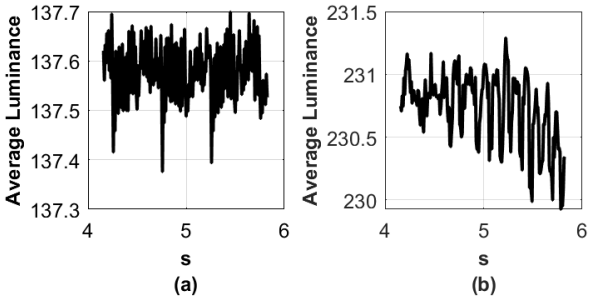

Figure 8. Average luminance at 12.5 m and 10% modulation (a) for the full frame and (b) spatially filtering to just the lights.

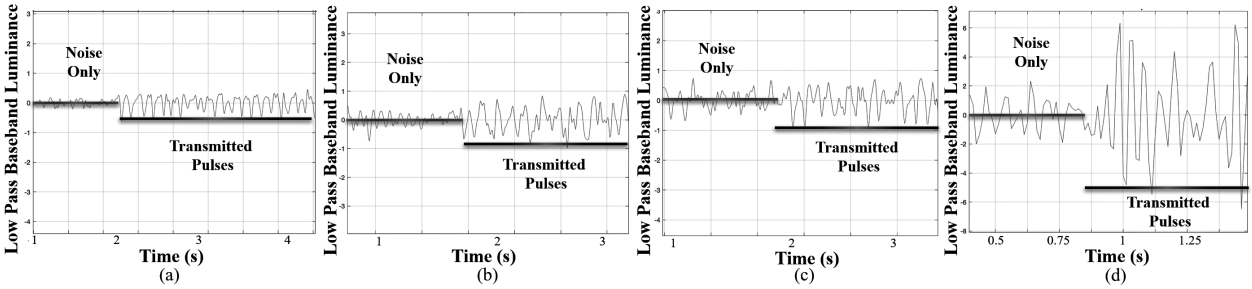

Figure 9. Received energy after lowpass filter and shift to baseband by removing running average at (a) 12.5 m, (b) 25 m, (c) 50 m, and (d) 100 m.

Having applied basic spatial filtering, the running average was removed from the signals and a low pass filter was applied before using peak detection for the symbol recovery algorithm. Figure 9 shows the conditioned signals at (a) 12.5 m, (b) 25 m, (c) 50 m, and (d) 100 m. The relative amplitude of noise in the signal can be clearly seen increasing as the range increases, which ultimately leads to lower SNR and an increased symbol error rate. These results are in line with expectations discussed in Section 2.2 and visualized in Figure 3.

Figure 10 shows the average results of three trial runs testing with a 10% modulation index at the various ranges previously outlined in Section 3.3. At 25 m, all symbols were recovered. At 50 and 100 m, 10% symbol error was encountered, jumping to 20% symbol error at 140 and 192 m. The process of decoding MPPM symbols, 4 pulses per 26 time slots, added robustness through maximum likelihood detection but also produced big quantization jumps in symbol errors per distance. Fitting a trend line to this data shows an increasing error rate of 0.012 symbols per meter. These results are consistent with most previous work in VLC limiting ranges to under 50 m, but also suggest that with further forward error correction, low data rate communication is plausible to at least 100 m without other optical optimization.

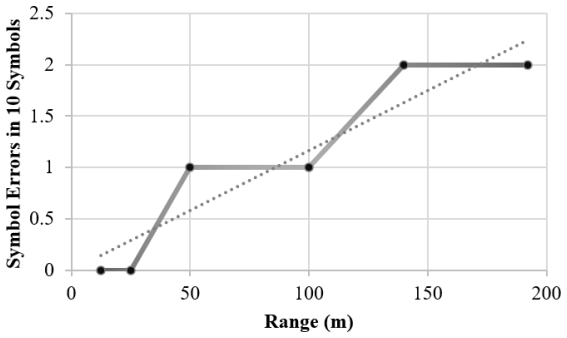

Figure 10. Symbol errors in ten symbols at varying ranges between transmitters and camera.

4.2. Effects of Varying Modulation Index

Having observed the criticality of spatial filtering and the numerous factors degrading symbol throughput with increasing range, further tests examined the effect of increasing the intensity modulation delta. We began by reducing the transmitted brightness by 8% to transmit a pulse in the MPPM scheme and gradually increased how deeply dimmed each pulse was for the whole series as laid out in Section 3.3. Illustrative of the results, Figure 11 shows the processed received signal at 100 m with (a) 8% dimming per pulse, (b) 16% dimming, (c) 48% dimming, and finally, (d) 100% dimming with the LED completely off to indicate a pulse.

We had previously seen that at 10% modulation, a 10% symbol error rate could be achieved at 100 m. From this exemplar subset, increasing the modulation depth makes the pulse much clearer as the difference in signal begins to dwarf the random noise variations at 48% modulation, and continuing to 70 or 100% modulation provides little to no gain. Conversely, as modulation depth increased, the range at which flicker was perceptible to human vision increased. Above 36% modulation, some flicker was detectable and, at 100% modulation, it was clearly blinking, even observing it from 100 m away.

While our data set had limited trials at the varying intensity modulations, using MPPM with spatial filtering symbol error rate remained around 10% at 50 m until reaching an intensity modulation delta of 54%, at which point no further symbol errors were observed. Results at 100 m experienced even greater noise variation, averaging out to a 10% symbol error rate with no symbol errors at 48% modulation and then a 20% symbol error rate at 54% modulation. However, using 100% modulation, no symbol errors were observed at 100 m.

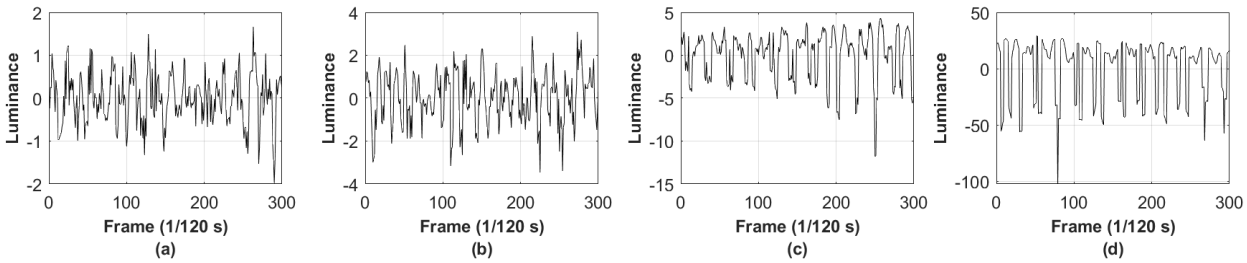

Figure 11. Processed signal received at 100 m with modulation depth of (a) 8%, (b) 16%, (c) 48%, and (d) 100%.

5. Conclusions

In this paper, we provided an outline of the numerous factors impacting outdoor VLC at increasing distances as well as documenting empirical test results with an exemplar V2V VLC set up and ranges nearing 200 m.

5.1. Findings

Many factors, spanning camera sensor processing and optics to propagation losses and atmospheric noise create challenges for increasing the range of VLC in daylight. Even in a clean signal with baseline drift removed, as seen in Figure 11(d), significant noise can be seen riding on top of the signal. As with all wireless communication, SNR is the critical driver to throughput and we have shown the effects of decreasing signal and increasing noise as distance increases.

Despite these challenges to outdoor VLC at increasing distances, using MPPM and spatial filtering, noise was sufficiently constrained to allow serviceable error rates for low data rate communications at 100 m. Considering V2V applications, this is approaching a desired range, noting that the stopping distance for a car traveling 100 km/h in optimal conditions is 50 m. Increasing intensity modulation further improved throughput, at a trade off of increased visible flicker, allowing very low error rates at distances up to 100 m.

5.2. Future Work

For critical messages, such as traffic being stopped ahead, a very low error rate and low latency are demanded. By increasing the depth of intensity modulation, we found errors can be eliminated at these ranges, with a trade-off of increased flicker in the system. Noting that no errors in transmission occurred at 100 m with 100% intensity modulation, an opportunity for future exploration is frequency shift keying in outdoor VLC. By encoding pulses in frequency changes while maintaining a constant brightness with the duty cycle, it may be possible to minimize both error rate and perceptible flicker.

Other future work can address specific limitations of OCC seen in Section 4.1. Enhanced optical zoom may help increase the area of the sensor illuminated by signal-containing pixels. Directly accessing raw CMOS data in the camera before sub-pixel mixing or other software optimizations may also help mitigate some aspects of camera induced noise.

References

Apple. (2021). *iPhone 13 Pro and 13 Pro Max - technical specifications*. https://www.apple.com/iphone-13-pro/specs/ (accessed: 06.05.2022)

Avatamanitei, S.-A., Cailean, A.-M., Done, A., Dimian, M., Popa, V., & Prelipceanu, M. (2020). Design and intensive experimental evaluation of an enhanced visible light communication system for automotive applications. *Sensors (Basel, Switzerland)*, *20*(11), 3190–.

Cailean, A.-M., & Dimian, M. (2016). Toward environmental-adaptive visible light communications receivers for automotive applications: A review. *IEEE sensors journal*, *16*(9), 2803–2811.

Cailean, A.-M., & Dimian, M. (2017). Current challenges for visible light communications usage in vehicle applications: A survey. *IEEE Communications surveys and tutorials*, *19*(4), 2681–2703.

Chowdhury, M. Z., Hossan, M. T., Islam, A., & Jang, Y. M. (2018). A comparative survey of optical wireless technologies: Architectures and applications. *IEEE Access*, *6*, 9819–9840. https://doi.org/10.1109/ACCESS.2018.2792419

Danakis, C., Afgani, M., Povey, G., Underwood, I., & Haas, H. (2012). Using a CMOS camera sensor for visible light communication. *2012 IEEE Globecom Workshops*, 1244–1248.

Federal Motor Vehicle Safety Standards; V2V communications (tech. rep.) [Copyright (c) 2017 Federal Information & News Dispatch, Inc; Last updated - 2017-01-12]. (2017). Federal Information & News Dispatch, LLC.

Ghassemlooy, Z., Popoola, W., & Rajbhandari, S. (2019). *Optical wireless communications: System and channel modelling with MATLAB®, second edition*. CRC Press.

Institute of Electrical and Electronics Engineers. (2010). IEEE standard for information technology– local and metropolitan area networks– specific requirements– part 11: Wireless LAN medium access control (MAC) and physical layer (PHY) specifications amendment 6: Wireless access in vehicular environments. *IEEE Std 802.11p-2010 (Amendment to IEEE Std 802.11-2007 as amended by IEEE Std 802.11k-2008, IEEE Std 802.11r-2008, IEEE Std 802.11y-2008, IEEE Std 802.11n-2009, and IEEE Std 802.11w-2009)*, 1–51. https://doi.org/10.1109/IEEESTD.2010.5514475

Ji, P., Tsai, H.-M., Wang, C., & Liu, F. (2014). Vehicular visible light communications with led taillight and rolling shutter camera. *2014 IEEE 79th Vehicular Technology Conference (VTC Spring)*, 1–6.

Koss, S., McAbee, C., Tummala, M., & McEachen, J. (2020). Symbol generation and frame synchronization for multipulse-pulse position modulation over optical channels. *2020 14th International Conference on Signal Processing and Communication Systems (ICSPCS)*, 1–7.

Lourenco, N., Terra, D., Kumar, N., Alves, L. N., & Aguiar, R. L. (2012). Visible light communication system for outdoor applications. *2012 8th International Symposium on Communication Systems, Networks & Digital Signal Processing (CSNDSP)*, 1–6.

Rajagopal, S., Roberts, R. D., & Lim, S.-K. (2012). IEEE 802.15.7 visible light communication: Modulation schemes and dimming support. *IEEE Communications Magazine*, *50*(3), 72–82. https://doi.org/10.1109/MCOM.2012.6163585

Rizzo, M. D., Song, D., Klingler, T. A., & Howland, D. L. (2011). Light vehicle dry stopping distance - vehicle speed correction, tire burnish, and surface friction correction. *SAE International journal of passenger cars. Mechanical systems*, *4*(1), 763–771.

Sanyal, R. (2021). *All Apple iPhone 13 and 13 Pro camera upgrades: Explained*. https://www.dpreview.com/articles/6780391159/all-apple-iphone-13-and-13-pro-camera-upgrades-explained (accessed: 06.05.2022)

Shannon, C. E. (1948). A mathematical theory of communication. *Bell System Technical Journal*, *27*(4), 623–656.

Shortis, M. R., Seager, J. W., Harvey, E. S., & Robson, S. (2005). Influence of Bayer filters on the quality of photogrammetric measurement. *Proc. SPIE*, *5665*(1), 164–171.

Teli, S., & Chung, Y.-H. (2018). Selective capture based high-speed optical vehicular signaling system. *Signal processing. Image communication*, *68*, 241–248.

Velidi, R., & Georghiades, C. (1995). Frame synchronization for optical multi-pulse pulse position modulation. *IEEE Transactions on Communications*, *43*(2/3/4), 1838–1843. https://doi.org/10.1109/26.380235

White, Z., Barber, D., Tummala, M., & McEachen, J. (2022). *A transmit diversity scheme for multipulse-pulse position modulated visible light communications*.

Yamazato, T., Kinoshita, M., Arai, S., Souke, E., Yendo, T., Fujii, T., Kamakura, K., & Okada, H. (2015). Vehicle motion and pixel illumination modeling for image sensor based visible light communication. *IEEE journal on selected areas in communications*, *33*(9), 1793–1805.

Yoo, J.-H., Jang, J.-S., Kwon, J. K., Kim, H.-C., Song, D.-W., & Jung, S.-Y. (2016). Demonstration of vehicular visible light communication based on LED headlamp. *International journal of automotive technology*, *17*(2), 347–352.